Phys. Lett. B 848 (2024) 138385

Contents lists available at ScienceDirect

Physics Letters B

journal homepage: www.elsevier.com/locate/physletb

Letter

Atomic masses with machine learning for the astrophysical *r* process

Mengke Li [a,*], Trevor M. Sprouse [b,c], Bradley S. Meyer [a], Matthew R. Mumpower [b,c]

[a] Department of Physics and Astronomy, Clemson University, Clemson, 29634, SC, USA
[b] Theoretical Division, Los Alamos National Laboratory, Los Alamos, 87545, NM, USA
[c] Center for Theoretical Astrophysics, Los Alamos National Laboratory, Los Alamos, 87545, NM, USA

ARTICLE INFO

Editor: B. Balantekin

Keywords:
Atomic mass model
Machine learning
r Process
Neutron star mergers
Nuclear properties
Error propagation

ABSTRACT

The astrophysical *r* process plays a vital role in the production of heavy elements. Modeling of the *r* process is sensitive to masses and further requires knowledge of masses beyond current experimental reach. Therefore, simulations of the *r* process offer a unique test bed for predicting mass extrapolations. We take a Machine-Learning (ML) approach to model the masses across the entire chart of nuclides. For the first time, we simulate *r*-process nucleosynthesis with a physics-based ML mass model. We compare simulated abundances to solar data in order to evaluate the model's performance far from stability. The resulting *r*-process abundances up to thorium and uranium qualitatively match those of the observed solar system abundance pattern, with the characteristic peaks well positioned. We propagate the mass uncertainties obtained from the ML model to *r*-process abundance yields to estimate an uncertainty band associated with our approach. The size of the uncertainty band is approximately one order of magnitude which aligns with the uncertainty reported using alternative techniques.

1. Introduction

The synthesis of heavy elements in our universe is a difficult interdisciplinary question. The astrophysical rapid neutron capture process (*r* process) is believed to be responsible for creating half of the heavy isotopes up to bismuth and all of thorium and uranium in our Universe [5]. To describe the *r*-process nucleosynthesis, uncertainties from two sources need to be well understood.

For astrophysical sites, there are many viable places that provide the necessary conditions for the *r* process, contributing to the overall abundance of *r*-process elements in the Galaxy. Collapsars were first proposed and studied by MacFadyen and Woosley in the 1990s [22]. Several groups performed detailed studies of nucleosynthesis in rapidly rotating core collapse [25,27,39]. NSMs as the production sites are expected theoretically [15,18]) and confirmed by the observed gravitational wave in GW170817 [1,37]. Analysis of the kilonovae that accompanied GW170817 identified delayed outflows from a remnant accretion disk as the important source of heavy *r*-process material [8,40,50]. Neutrino-driven wind (NDW) is also a favored model for *r*-process nucleosynthesis for years. Although, Refs. [12,47] have found the NDW to be inadequate as an *r*-process site, Ref. [43] shows that the Magnetic Neutrino-Driven Wind can be an appropriate condition for the *r*-process nuclei creation. In addition, studies from Refs. [7,38] demonstrate that mergers of a black hole and a neutron star can also eject extremely neutron-rich materials that allow the *r* process to occur. Magneto-rotational hypernovae reported in Ref. [51] and magneto-hydrodynamic jet supernovas in Ref. [34] may also be candidate sites. The astrophysical conditions vary dramatically in these environments and are thus one source of uncertainty in simulating heavy element formation.

Nuclear properties play another influential role in the *r* process. In particular, atomic masses are used in the computation of all nuclear transmutations (neutron capture rates, photo-dissociation rates, β-decay rates, etc.). Around 2500 nuclei have been measured experimentally. However, more than 7000 isotopes are predicted to exist in the nuclear landscape [9]. Therefore, it is imperative to produce reliable theoretical predictions for atomic masses. Tremendous efforts have been made in developing nuclear mass models, e.g., KTUY model [16], Finite Range Droplet Model (FRDM) [28], Duflo–Zuker (DZ) [49], and Hartree–Fock–Bogoliubov (HFB) model [11]. All of these models give a reasonable fit to known experimental masses, however deviations between model predictions rapidly grow in neutron-rich nuclei that participate in the *r* process.

With recent advances in computation, Machine Learning (ML) has been widely applied with success in many fields. In recent nuclear mass studies, networks have been trained on reducing the differences

* Corresponding author.
E-mail address: mengkel@g.clemson.edu (M. Li).

https://doi.org/10.1016/j.physletb.2023.138385
Received 2 August 2023; Received in revised form 8 November 2023; Accepted 4 December 2023
Available online 6 December 2023

Table 1
Input features in Mixture Density Network.

Features	Description
N	Neutron number
Z	Proton number
A	Mass number
P_{asym}	Asymmetry correction
V_n	Valence neutron
V_p	Valence proton
N_{eo}	Evenness and oddness of neutron number
Z_{eo}	Evenness and oddness of proton number
A_{eo}	Evenness and oddness of mass number
$V_n + V_p$	Sum of valence neutron and proton
$V_n * V_p$	Multiplication of valence neutron and proton
$\frac{V_n+V_p}{V_n*V_p}$	Proton neutron interactions

between the Atomic Mass Evaluation and various mass models [33]. Ref. [44] used a Bayesian Neural Network (BNN) approach to refine the predictions of existing mass models. Ref. [35] explored the BNN method in predicting the masses when nuclear pairing and shell effects are included. Ref. [10] investigated a Light Gradient Boosting Machine algorithm in predicting the nuclear mass with a large training set (80% of AME data). A Mixture Density Network (MDN) has been used [20,32] to predict the masses of nuclei with well-quantified uncertainties.

In this work, we explore for the first time the impacts of a ML-based mass model on the astrophysical *r*-process abundances. We propagate the mass predictions to the astrophysical *r*-process by computing one neutron separation energies. We assess the quality of the extrapolations by comparing the simulated *r*-process abundance pattern to solar data. The ML model estimates uncertainties and it naturally encodes correlations among input. We use these properties to self-consistently estimate abundance uncertainties with this method.

2. Methods

We used a probabilistic Machine Learning technique, the MDN [4], to train a mass model. Our probabilistic network is written in PyTorch [36] and can be implemented on either CPU or GPU architectures. Ref. [21] showed that this algorithm is able to describe nuclear properties with well-quantified uncertainties. The model encodes the physical information in the feature space to increase the accuracy of atomic mass predictions [20,35]. When the feature space combines macroscopic and microscopic terms, it is suitable for describing masses across the chart of nuclides [32]. The use of hybrid training data, consisting of high precision evaluation data and low precision theoretical data, can improve the extrapolation quality [31].

Based on these previous studies, we developed a new mass model adding proton-neutron interaction terms related to nuclear promiscuity into the feature space [6]. The input features are listed in Table 1.

The training set in our model is a random selection of 600 nuclei from Atomic Mass Evaluation (AME2020) reported in Ref. [48] with Z $\geq$ 10. To give our model more physical information to enhance the predictive power, similar to our previous work [31], we randomly chose 50 theoretical mass data that are not available in AME2020, from a well-accepted mass model HFB-32, as extra training samples. This extra bit of theoretical information helps the model to anchor the predictions, so they do not stray too far from expected physics. Fig. 1 shows the training data in this work. It consists of 650 nuclei (23% of AME2020) shown in blue, and the extra data shown in red.

Training of the ML model follows the steps in Refs. [31,32]. Our neural network architecture comprises six hidden layers, with ten hidden nodes in each layer. The hyperbolic tangent function is used as the activation function for neurons in the linear network, while a softmax function is employed in the final layer. A learning rate scheduler is employed that takes the initial learning rate times 0.65 for every 10,000 epochs up to 100,000 epochs which stabilizes the neural network performance. The total loss $\mathcal{L}_{total} = \mathcal{L}_1 + \lambda_{phys}\mathcal{L}_2$ is minimized

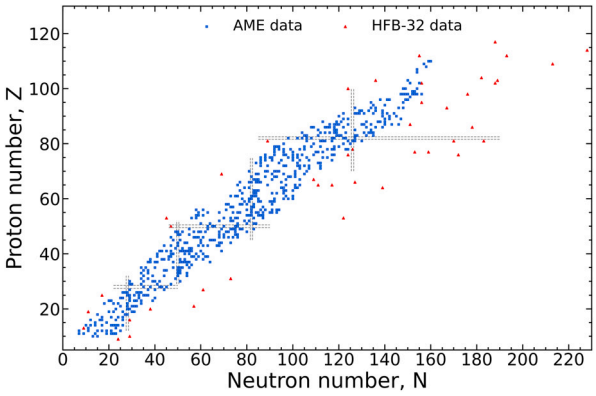

Fig. 1. The training data set is shown. Blue squares are the 600 nuclei selected from the AME2020, while the red ones are theoretical data samples from the HFB-32 mass model. The dashed gray lines show the proton and neutron closed shells for reference.

in the training process, where $\mathcal{L}_1$ is the match to the AME data, and $\mathcal{L}_2$ is a physics constraint with $\lambda_{phys} = 0.3$. The training process is terminated when the total loss function achieves its minimum value and remains stable thereafter. The output of this model is a set of predicted atomic masses $M(Z,N)$ with their corresponding standard deviations $\sigma_M(Z,N)$.

To explore the impacts of masses on *r*-process simulations, we calculate the neutron separation energy as:

$$S_{\rm n}(Z,N) = M(Z,N-1) + m_n - M(Z,N)\,, \tag{1}$$

where m_n is the mass of the neutron. The standard deviation of $S_{\rm n}$ coming from the uncertain masses is calculated by:

$$\sigma_{S_{\rm n}} = \sqrt{\sigma_M^2(Z,N-1) + \sigma_M^2(Z,N)}\,, \tag{2}$$

where it has been explicitly assumed that the uncertainties between mass predictions are uncorrelated.

3. Results

3.1. Atomic masses

We compared our mass model predictions to the entire AME2020 dataset. The root-mean-square (RMS) error was approximately 138 keV for the training set, which covered 23 percent of AME2020, and approximately 246 keV when calculated against the AME2020 dataset with Z $\geq$ 10. Our results are competitive with contemporary theoretical models currently available. We tested our model without including any additional theoretical data samples and found it difficult to reduce the testing RMS below 300 keV. We conclude that incorporating a small set of theoretical data samples from a mass model (HFB-32) in the training process can improve the overall fit of the observed atomic mass data.

3.2. Extrapolation in S_n

The one neutron separation energy ($S_{\rm n}$) is the energy required to remove one neutron from a nucleus. It holds significant importance in both nuclear physics and astrophysics [14,24]. In terms of nuclear structure, $S_{\rm n}$ is relevant to closed-shell, pairing effects, and the boundaries of the nuclear landscape. In astrophysics, $S_{\rm n}$ sets the equilibrium *r*-process path through the calculation of the photo-dissociation rate via detailed balance. Many studies have shown that $S_{\rm n}$ is of great significance in understanding the simulated abundance pattern in different evolution phases [17].

Fig. 2 displays the $S_{\rm n}$ for Lead (Z=82) isotopes. The predictions from the ML model, which are shown in blue, are in good agreement

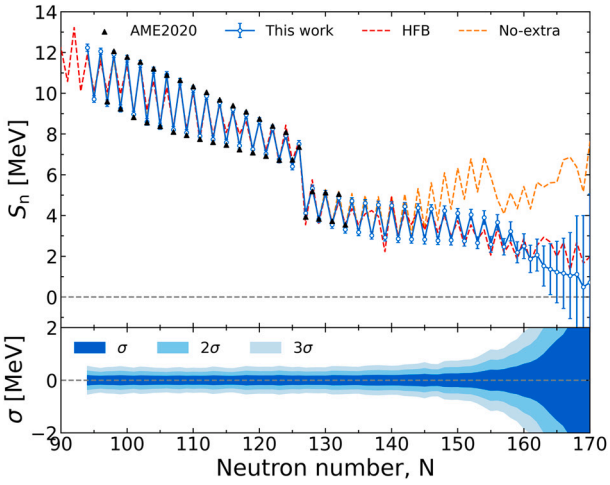

Fig. 2. The upper panel of the figure compares the S_n values in the Pb isotopic chain obtained from experimental data (represented by black triangles), the mass model discussed in this work (represented by blue circles), the HFB model (represented by red dashed line), and the machine learning model without additional theoretical data samples (represented by dashed orange line). The error bars associated with the blue circles show the standard deviation of each calculated S_n as calculated using Equation (2). The blue line connecting the blue circles emphasizes the odd-even staggering in the data. The lower panel illustrates the 1-3 σ uncertainties of each calculated S_n using gradually lighter blue bands.

with experimental data where available. The model's extrapolation remains physically valid as evident by the general declining trend of S_n with increasing neutron number and the odd-even staggering observed throughout the isotopic chain. This phenomenon can be observed in every isotopic chain and provides the first indication that the extrapolation of mass and neutron separation energy from our ML-based mass model remains reliable in neutron-rich regions.

To provide a comparative analysis, we include predictions from two alternative models. The first is the HFB-32 mass model shown in red, which exhibits similar trends to our model with minor deviations. The second model, trained with the same parameters but without the HFB-32 data samples in the training data set, which is labeled "No-extra" in Fig. 2, displays a nonphysical increasing trend in neutron separation energy as the neutron number increases. The disparity between the blue and orange curves highlights the benefits of incorporating suggestive data samples from theory, as it enhances the performance of our model in extrapolations.

To quantify the uncertainties of the extrapolated S_n, the lower panel of Fig. 2 illustrates the 1-3 σ of each calculated S_n using gradually lighter blue bands respectively. The uncertainties grow as a function of neutron richness, and begin to rapidly increase around the neutron dripline.

In Fig. 3, we compare the mass predictions of the ML model against those of the HFB-32 model, highlighting their deviations. While both models align closely in the experimentally available region (enclosed by the black contour line), discrepancies emerge in the neutron-rich areas, providing a testable difference between these two predictions.

3.3. Application to r-process nucleosynthesis

Observed features in *r*-process abundance pattern arise from the interplay of nuclear masses, β-decay, and neutron capture rates with appropriate astrophysical conditions. To study the impacts of our mass model in the astrophysical *r*-process, we incorporate the atomic mass predictions into *r*-process nucleosynthesis simulations and then compare the resulting abundance patterns with the observed solar system abundance data. We simulate nucleosynthesis using the nuclear reaction network code PRISM [30]. In our simulations, we calculate photo-

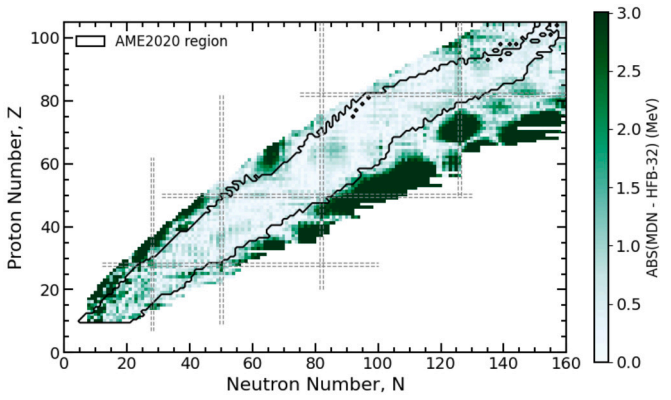

Fig. 3. Predicted mass deviations between the ML model and the HFB-32, illustrated using a color-map to depict the absolute differences. Within each isotopic chain, only isotopes preceding the neutron drip-line are shown. The black contour line delineates the region with available experimental data, while the dashed gray lines indicate the proton and neutron closed shells for reference.

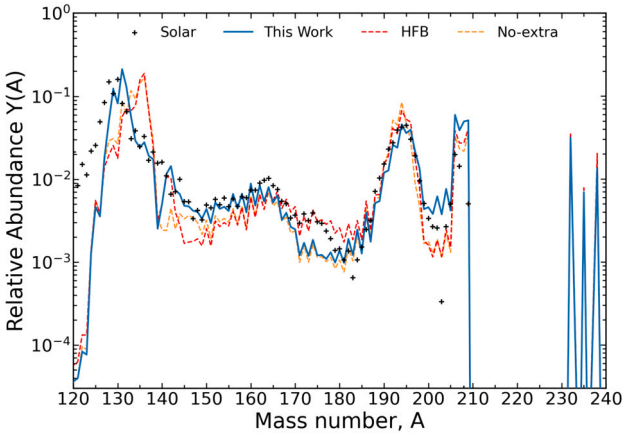

Fig. 4. Abundance patterns Y (A) versus A for three *r*-process simulations with astrophysical condition corresponding to dynamical ejecta. The blue curve uses the mass model developed in this work. For comparison, the red dashed pattern corresponds to the HFB-32 mass model, while the orange dashed one is using a similar machine learning model trained without extra theoretical data samples. All patterns are scaled to solar abundances reported in Ref. [2] with black cross signs.

dissociation rates via detailed balance using separation energies from our mass model. The neutron capture and beta-decay rates remain unchanged as in the above citations. We probe two distinct astrophysical trajectories, the wind ejecta of Ref. [52] and the dynamical ejecta of Ref. [26]; the latter exhibits robust fission recycling. To focus the analysis on the behavior of our mass model, we use a 50–50 split when nuclei undergo fission so that this interaction does not mask interesting features that may arise from the use of our masses [46].

The simulated *r*-process abundance patterns at 1 Gyr are shown in Fig. 4 for dynamical ejecta conditions. The blue curve uses the ML mass model described in this work. Overall, the final abundances using the ML model match well with the solar isotopic residuals.

Under these conditions, the two prominent *r*-process peaks attributed to closed neutron shells at $A = 130$ ($N = 82$) and $A = 195$ ($N = 126$) are well reproduced. It is interesting to note that the ML model predicts a relatively weaker closed shell at $N = 126$. This can be measured by the $N = 126$ shell gap tending towards zero faster than other models in the literature. As a consequence, more material passes through to the actinide region and produces a relatively higher lead region peak around $A \sim 208$.

In contrast to the main peaks, when it comes to matching the rare earth peak around $A \sim 165$, which is believed to form via a different

nuclear structure mechanism Ref. [42], our ML model does not perform as well. While our simulation shows a close agreement with the left edge of the peak, there is a noticeable deviation at the top of the peak and along the right edge. This discrepancy could potentially be attributed to the predicted atomic masses in highly deformed nuclei that are thought to be responsible for peak formation [45]. The rare earth peak remains a challenging feature to reproduce in the solar pattern [13] and matching it will likely only be resolved by the inclusion of future precision mass measurements in the region.

To contrast our ML model's extrapolation quality, we conduct a second *r*-process simulation with the only change being separation energies now calculated from the HFB-32 mass model, depicted by the dashed red curve. Comparing the results of both simulations, we find that the $A = 130$ peak is better reproduced with the ML masses than HFB-32, whereas the right edge of the rare earth peak is more inline with HFB-32 than the ML model.

Finally, we also compare to an *r*-process simulation using the ML masses without the additional theoretical data in training (indicated in orange and labeled as "No-extra"). Notably, the model fails to accurately match the second peak abundance, similar to the behavior of HFB-32. Generally, we find that the resulting abundance pattern is comparable to the blue curve for $A > 165$ and approaches the red curve for $A < 165$. This situation arises due in part to the unphysical behavior found along some mass chains as shown in Fig. 2. The variability across mass ranges of different features suggests that it may be difficult to extract the behavior of masses of neutron-rich isotopes from a global match to solar data alone.

3.4. Uncertainty propagation of ML masses to r-process abundances

To explore the error in our simulated abundances arising from uncertainties in our method, we propagate the changes in predicted separation energies for a 1000 samples of our ML mass model. For each individual mass set, we sample the atomic masses with a probability distribution,

$$P(m) = \frac{1}{\sigma_i \sqrt{2\pi}} e^{-\frac{1}{2}(\frac{m-\mu_i}{\sigma_i})^2}, \tag{3}$$

where μ_i and σ_i are the predicted mass and corresponding uncertainty of each nucleus from our mass model, while m is the sampled mass data. The mass changes are used to construct separation energies, and the *r* process is simulated as above. The error bands for the two astrophysical scenarios are shown in Fig. 5. The top panel shows the behavior of these samples for dynamical ejecta while the bottom panel shows the behavior of the samples for the wind ejecta. The former is well behaved and generally follows the solar pattern while deviations are seen in the case of the wind ejecta. From the lower panel, we observe a much stronger rare earth peak structure than in the case of dynamical ejecta. The poor performance in this scenario could indicate that the features of this ML mass model are too strongly weighting the local fluctuations of deformed nuclei in training.

In both conditions, the abundance error band spans roughly one order in magnitude. The size of this band is consistent with the use of other theoretical models, as reported in Refs. [23] and [41]. This observation differs from the findings of Ref. [29]. The latter study implemented a Monte Carlo mass variation approach, where a fixed significant uncertainty range was applied to all nuclei, resulting in the generation of relatively larger uncertainty bands. In contrast, the uncertainties in this work steadily grow as a function of neutron excess (recall Fig. 2), providing a more reliable picture of the associated uncertainties.

3.5. β-decay heating rates

Our ML-driven mass models facilitate the computation of mass differences and their associated Q values. These quantities are pivotal for the accurate determination of nuclear heating rates which are a critical component in the analysis of kilonovae events [19]. To assess the uncertainties stemming from our predictions, we compute the β-decay energy release associated with each mass model's r-process simulation. The resultant heating rates are shown in Fig. 6, where the breadth of the green band encapsulates the extent of the uncertainties. It is important to note that this green band arises from unmeasured, short-lived masses far from stability, even though the masses of nuclei that are populated at a specific time are well measured in this figure. Another way to say this is that uncertainties in short-lived properties accumulate to cause a spread in quantities that may be observed on longer timescales. We find that the band is smaller than the relatively large deviations found between various nuclear models explored in the past work of Refs. [3,53] because the masses probed by our ML model are inherently correlated.

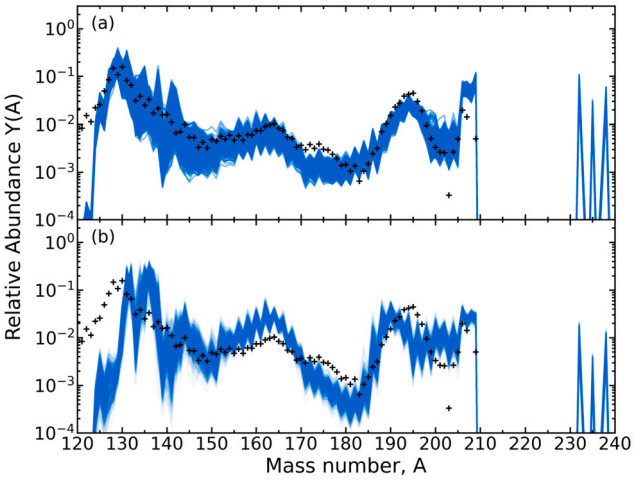

Fig. 5. Abundance patterns Y (A) versus A for 1000 *r*-process simulations with astrophysical conditions corresponding to dynamical ejecta (a), wind ejecta (b), from binary neutron star mergers. Each light blue line is a simulation with one mass set sampled by Monte Carlo method. All patterns are scaled to solar abundances with black cross signs.

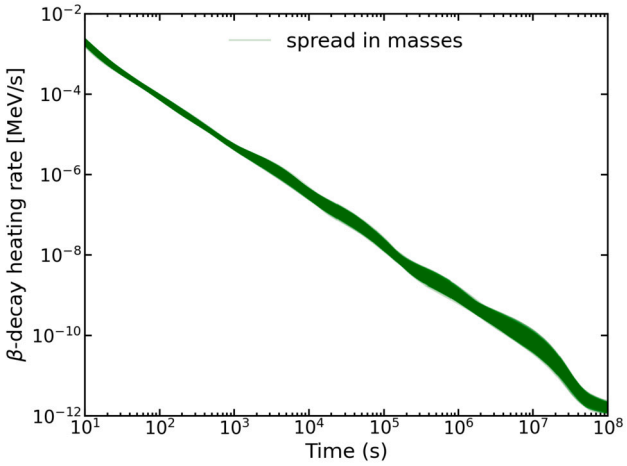

Fig. 6. β-decay heating rate vs. time for the 1000 mass sets. The green band indicates the spread in the heating rate arising from the uncertainty in short-lived masses.

4. Conclusions and discussions

We have developed a Machine Learning mass model based on the Mixture Density Network. This ML model predicts atomic masses and associated uncertainties across the chart of nuclides. Physical behavior

of important quantities such as the neutron separation energy is found to be retained as a function of neutron excess.

To more concretely gauge the extrapolation quality of this model, it is employed in *r*-process simulations, which are extremely sensitive to the mass of short-lived nuclei. It is found that the ML-based model performs on par with other established theoretical models in the literature. The predicted masses are tested in two distinct astrophysical conditions: dynamical ejecta and wind ejecta. The second and third *r*-process peaks are well positioned for these astrophysical conditions and the overall fit is found to be better in dynamical ejecta as compared to wind ejecta when comparing the simulated abundances to solar data. We self-consistently calculate the errors associated with our predicted abundances and find them in line with other estimates in the literature: on average one order of magnitude or less.

Our study is the first to show that ML-based models can be used in extrapolating masses that are key inputs for *r*-process simulations. The success of our procedure in the prediction of ground state masses for neutron-rich nuclei far from current measurements gives credence to this methodology's applicability to other low-energy nuclear phenomenon, such as beta decay half-lives, reaction cross sections, and isomeric states. Furthermore, our work extends the functionality of ML mass models to the determination of mass differences and associated Q values, which are critical in the prediction of heating rates used in the calculation of kilonova light curves. This advancement lays the groundwork for future ML studies of more complex phenomena in astrophysics.

Our technique for generating ML-based models is driven primarily by precision data coupled with pertinent physical constraints. Therefore, future measurements will further enable the power of this method as more nuclear data is produced by experimental facilities worldwide.

Declaration of competing interest

The authors declare that they have no known competing financial interests or personal relationships that could have appeared to influence the work reported in this paper.

Data availability

Data will be made available on request.

Acknowledgements

M.L., T.M.S., and M.R.M. are supported by the US Department of Energy through the Los Alamos National Laboratory (LANL). LANL is operated by Triad National Security, LLC, for the National Nuclear Security Administration of U.S. Department of Energy (Contract No. 89233218CNA000001). This research was supported by LANL through its Center for Space and Earth Science (CSES). CSES is funded by LANL's Laboratory Directed Research and Development (LDRD) program under project number 20210528CR. M.L. and B.S.M. were supported by NASA Emerging Worlds grant with grant number 80NSSC20K0338.

References

[1] B.P. Abbott, et al., LIGO Scientific Collaboration and Virgo Collaboration, Gw170817: observation of gravitational waves from a binary neutron star inspiral, Phys. Rev. Lett. 119 (2017) 161101, https://doi.org/10.1103/PhysRevLett.119.161101.

[2] M. Arnould, S. Goriely, K. Takahashi, The r-process of stellar nucleosynthesis: astrophysics and nuclear physics achievements and mysteries, Phys. Rep. 450 (2007) 97–213, https://doi.org/10.1016/j.physrep.2007.06.002.

[3] J. Barnes, Y.L. Zhu, K.A. Lund, T.M. Sprouse, N. Vassh, G.C. McLaughlin, M.R. Mumpower, R. Surman, Kilonovae across the nuclear physics landscape: the impact of nuclear physics uncertainties on r-process-powered emission, Astrophys. J. 918 (2021) 44, https://doi.org/10.3847/1538-4357/ac0aec.

[4] C. Bishop, Mixture density networks, Working paper, Aston University, 1994.

[5] E.M. Burbidge, G.R. Burbidge, W.A. Fowler, F. Hoyle, Synthesis of the elements in stars, Rev. Mod. Phys. 29 (1957) 547–650, https://doi.org/10.1103/RevModPhys.29.547.

[6] R.F. Casten, D.S. Brenner, P.E. Haustein, Valence p-n interactions and the development of collectivity in heavy nuclei, Phys. Rev. Lett. 58 (1987) 658–661, https://doi.org/10.1103/PhysRevLett.58.658.

[7] S. Curtis, J.M. Miller, C. Fröhlich, T. Sprouse, N. Lloyd-Ronning, M. Mumpower, Nucleosynthesis in outflows from black hole-neutron star merger disks with full GR(ν)RMHD, Astrophys. J. Lett. 945 (2023) L13, https://doi.org/10.3847/2041-8213/acba16, arXiv:2212.10691.

[8] B. Côté, C.L. Fryer, K. Belczynski, O. Korobkin, M. Chruślińska, N. Vassh, M.R. Mumpower, J. Lippuner, T.M. Sprouse, R. Surman, R. Wollaeger, The origin of r-process elements in the Milky Way, Astrophys. J. 855 (2018) 99, https://doi.org/10.3847/1538-4357/aaad67.

[9] J. Erler, N. Birge, M. Kortelainen, W. Nazarewicz, E. Olsen, A.M. Perhac, M. Stoitsov, The limits of the nuclear landscape, Nature 486 (2012) 509–512, https://doi.org/10.1038/nature11188.

[10] Z. Gao, Y. Wang, H. Lü, Q. Li, C. Shen, L. Liu, Machine learning the nuclear mass, arXiv e-prints, arXiv:2105.02445, 2021.

[11] S. Goriely, N. Chamel, J.M. Pearson, Further explorations of Skyrme-Hartree-Fock-Bogoliubov mass formulas. XVI. Inclusion of self-energy effects in pairing, Phys. Rev. C 93 (2016) 034337, https://doi.org/10.1103/PhysRevC.93.034337.

[12] L. Hüdepohl, B. Müller, H.T. Janka, A. Marek, G.G. Raffelt, Neutrino signal of electron-capture supernovae from core collapse to cooling, Phys. Rev. Lett. 104 (2010) 251101, https://doi.org/10.1103/PhysRevLett.104.251101.

[13] X.F. Jiang, X.H. Wu, P.W. Zhao, Sensitivity study of r-process abundances to nuclear masses, Astrophys. J. 915 (2021) 29, https://doi.org/10.3847/1538-4357/ac042f.

[14] T. Kajino, W. Aoki, A.B. Balantekin, R. Diehl, M.A. Famiano, G.J. Mathews, Current status of r-process nucleosynthesis, Prog. Part. Nucl. Phys. 107 (2019) 109–166, https://doi.org/10.1016/j.ppnp.2019.02.008, arXiv:1906.05002.

[15] O. Korobkin, S. Rosswog, A. Arcones, C. Winteler, On the astrophysical robustness of the neutron star merger r-process, Mon. Not. R. Astron. Soc. 426 (2012) 1940–1949, https://doi.org/10.1111/j.1365-2966.2012.21859.x, https://academic.oup.com/mnras/article-pdf/426/3/1940/3105409/426-3-1940.pdf.

[16] H. Koura, T. Tachibana, M. Uno, M. Yamada, Nuclidic mass formula on a spherical basis with an improved even-odd term, Prog. Theor. Phys. 113 (2005) 305–325, https://doi.org/10.1143/PTP.113.305, https://academic.oup.com/ptp/article-pdf/113/2/305/5192381/113-2-305.pdf.

[17] M. Li, B.S. Meyer, Dependence of $(n,\gamma)-(\gamma,n)$ equilibrium *r*-process abundances on nuclear physics properties, Phys. Rev. C 106 (2022) 035803, https://doi.org/10.1103/PhysRevC.106.035803.

[18] J. Lippuner, R. Fernández, L.F. Roberts, F. Foucart, D. Kasen, B.D. Metzger, C.D. Ott, Signatures of hypermassive neutron star lifetimes on r-process nucleosynthesis in the disc ejecta from neutron star mergers, Mon. Not. R. Astron. Soc. 472 (2017) 904–918, https://doi.org/10.1093/mnras/stx1987, https://academic.oup.com/mnras/article-pdf/472/1/904/19717364/stx1987.pdf.

[19] J. Lippuner, L.F. Roberts, r-Process lanthanide production and heating rates in kilonovae, Astrophys. J. 815 (2015) 82, https://doi.org/10.1088/0004-637X/815/2/82.

[20] A.E. Lovell, A.T. Mohan, T.M. Sprouse, M.R. Mumpower, Nuclear masses learned from a probabilistic neural network, Phys. Rev. C 106 (2022) 014305, https://doi.org/10.1103/PhysRevC.106.014305.

[21] A.E. Lovell, A.T. Mohan, P. Talou, M. Chertkov, Quantified uncertainties in fission yields from machine learning, in: European Physical Journal Web of Conferences, 2020, p. 05003.

[22] A.I. MacFadyen, S.E. Woosley, Collapsars: gamma-ray bursts and explosions in "failed supernovae", Astrophys. J. 524 (1999) 262, https://doi.org/10.1086/307790.

[23] D. Martin, A. Arcones, W. Nazarewicz, E. Olsen, Impact of nuclear mass uncertainties on the *r* process, Phys. Rev. Lett. 116 (2016) 121101, https://doi.org/10.1103/PhysRevLett.116.121101.

[24] G. Martínez-Pinedo, K. Langanke, Nuclear quests for the r-process, Eur. Phys. J. A 59 (2023) 67, https://doi.org/10.1140/epja/s10050-023-00987-9.

[25] G. McLaughlin, R. Surman, Prospects for obtaining an r process from gamma ray burst disk winds, Nucl. Phys. A 758 (2005) 189–196, https://doi.org/10.1016/j.nuclphysa.2005.05.036, Nuclei in the Cosmos VIII.

[26] J.d.J. Mendoza-Temis, M.R. Wu, K. Langanke, G. Martínez-Pinedo, A. Bauswein, H.T. Janka, Nuclear robustness of the *r* process in neutron-star mergers, Phys. Rev. C 92 (2015) 055805, https://doi.org/10.1103/PhysRevC.92.055805.

[27] J.M. Miller, T.M. Sprouse, C.L. Fryer, B.R. Ryan, J.C. Dolence, M.R. Mumpower, R. Surman, Full transport general relativistic radiation magnetohydrodynamics for nucleosynthesis in collapsars, Astrophys. J. 902 (2020) 66, https://doi.org/10.3847/1538-4357/abb4e3.

[28] P. Möller, W.D. Myers, H. Sagawa, S. Yoshida, New finite-range droplet mass model and equation-of-state parameters, Phys. Rev. Lett. 108 (2012) 052501, https://doi.org/10.1103/PhysRevLett.108.052501.

[29] M. Mumpower, R. Surman, G. McLaughlin, A. Aprahamian, The impact of individual nuclear properties on *r*-process nucleosynthesis, Prog. Part. Nucl. Phys. 86 (2016) 86–126, https://doi.org/10.1016/j.ppnp.2015.09.001.

[30] M.R. Mumpower, T. Kawano, T.M. Sprouse, N. Vassh, E.M. Holmbeck, R. Surman, P. Möller, β-delayed fission in r-process nucleosynthesis, Astrophys. J. 869 (2018) 14, https://doi.org/10.3847/1538-4357/aaeaca, arXiv:1802.04398.

[31] M.R. Mumpower, M. Li, T.M. Sprouse, B.S. Meyer, A.E. Lovell, A.T. Mohan, Bayesian averaging for ground state masses of atomic nuclei in a machine learning approach, arXiv:2304.08546, 2023.
[32] M.R. Mumpower, T.M. Sprouse, A.E. Lovell, A.T. Mohan, Physically interpretable machine learning for nuclear masses, Phys. Rev. C 106 (2022) L021301, https://doi.org/10.1103/PhysRevC.106.L021301.
[33] L. Neufcourt, Y. Cao, S.A. Giuliani, W. Nazarewicz, E. Olsen, O.B. Tarasov, Quantified limits of the nuclear landscape, Phys. Rev. C 101 (2020) 044307, https://doi.org/10.1103/PhysRevC.101.044307.
[34] N. Nishimura, T. Takiwaki, F.K. Thielemann, The r-process nucleosynthesis in the various jet-like explosions of magnetorotational core-collapse supernovae, Astrophys. J. 810 (2015) 109, https://doi.org/10.1088/0004-637X/810/2/109.
[35] Z. Niu, H. Liang, Nuclear mass predictions based on Bayesian neural network approach with pairing and shell effects, Phys. Lett. B 778 (2018) 48–53, https://doi.org/10.1016/j.physletb.2018.01.002.
[36] A. Paszke, S. Gross, F. Massa, A. Lerer, J. Bradbury, G. Chanan, T. Killeen, Z. Lin, N. Gimelshein, L. Antiga, A. Desmaison, A. Kopf, E. Yang, Z. DeVito, M. Raison, A. Tejani, S. Chilamkurthy, B. Steiner, L. Fang, J. Bai, S. Chintala, Pytorch: an imperative style, high-performance deep learning library, in: H. Wallach, H. Larochelle, A. Beygelzimer, F. d'Alché-Buc, E. Fox, R. Garnett (Eds.), Advances in Neural Information Processing Systems, Curran Associates, Inc., 2019, https://proceedingsneuripscc/paper/2019/file/bdbca288fee7f92f2bfa9f7012727740-Paperpdf.
[37] E. Pian, P. D'Avanzo, S. Benetti, M. Branchesi, E. Brocato, S. Campana, E. Cappellaro, S. Covino, V. D'Elia, J.P.U. Fynbo, F. Getman, G. Ghirlanda, G. Ghisellini, A. Grado, G. Greco, J. Hjorth, C. Kouveliotou, A. Levan, L. Limatola, D. Malesani, P.A. Mazzali, A. Melandri, P. Møller, L. Nicastro, E. Palazzi, S. Piranomonte, A. Rossi, O.S. Salafia, J. Selsing, G. Stratta, M. Tanaka, N.R. Tanvir, L. Tomasella, D. Watson, S. Yang, L. Amati, L.A. Antonelli, S. Ascenzi, M.G. Bernardini, M. Boër, F. Bufano, A. Bulgarelli, M. Capaccioli, P. Casella, A.J. Castro-Tirado, E. Chassande-Mottin, R. Ciolfi, C.M. Copperwheat, M. Dadina, G. De Cesare, A. di Paola, Y.Z. Fan, B. Gendre, G. Giuffrida, A. Giunta, L.K. Hunt, G.L. Israel, Z.P. Jin, M.M. Kasliwal, S. Klose, M. Lisi, F. Longo, E. Maiorano, M. Mapelli, N. Masetti, L. Nava, B. Patricelli, D. Perley, A. Pescalli, T. Piran, A. Possenti, L. Pulone, M. Razzano, R. Salvaterra, P. Schipani, M. Spera, A. Stamerra, L. Stella, G. Tagliaferri, V. Testa, E. Troja, M. Turatto, S.D. Vergani, D. Vergani, Spectroscopic identification of r-process nucleosynthesis in a double neutron-star merger, Nature 551 (2017) 67–70, https://doi.org/10.1038/nature24298, arXiv:1710.05858.
[38] L.F. Roberts, J. Lippuner, M.D. Duez, J.A. Faber, F. Foucart, J.C. Lombardi Jr., S. Ning, C.D. Ott, M. Ponce, The influence of neutrinos on r-process nucleosynthesis in the ejecta of black hole–neutron star mergers, Mon. Not. R. Astron. Soc. 464 (2016) 3907–3919, https://doi.org/10.1093/mnras/stw2622, https://academic.oup.com/mnras/article-pdf/464/4/3907/8310076/stw2622.pdf.
[39] D.M. Siegel, J. Barnes, B.D. Metzger, Collapsars as a major source of r-process elements, Nature 569 (2019) 241–244, https://doi.org/10.1038/s41586-019-1136-0.
[40] D.M. Siegel, B.D. Metzger, Three-dimensional general-relativistic magnetohydrodynamic simulations of remnant accretion disks from neutron star mergers: outflows and *r*-process nucleosynthesis, Phys. Rev. Lett. 119 (2017) 231102, https://doi.org/10.1103/PhysRevLett.119.231102.
[41] T.M. Sprouse, R. Navarro Perez, R. Surman, M.R. Mumpower, G.C. McLaughlin, N. Schunck, Propagation of statistical uncertainties of Skyrme mass models to simulations of *r*-process nucleosynthesis, Phys. Rev. C 101 (2020) 055803, https://doi.org/10.1103/PhysRevC.101.055803.
[42] R. Surman, J. Engel, J.R. Bennett, B.S. Meyer, Source of the rare-earth element peak in **r**-process nucleosynthesis, Phys. Rev. Lett. 79 (1997) 1809–1812, https://doi.org/10.1103/PhysRevLett.79.1809.
[43] T.A. Thompson, A. ud-Doula, High-entropy ejections from magnetized proto-neutron star winds: implications for heavy element nucleosynthesis, Mon. Not. R. Astron. Soc. 476 (2018) 5502–5515, https://doi.org/10.1093/mnras/sty480, https://academic.oup.com/mnras/article-pdf/476/4/5502/24610989/sty480.pdf.
[44] R. Utama, J. Piekarewicz, Refining mass formulas for astrophysical applications: a Bayesian neural network approach, Phys. Rev. C 96 (2017) 044308, https://doi.org/10.1103/PhysRevC.96.044308.
[45] N. Vassh, G.C. McLaughlin, M.R. Mumpower, R. Surman, The need for a local nuclear physics feature in the neutron-rich rare-earths to explain solar *r*-process abundances, arXiv:2202.09437, 2022.
[46] N. Vassh, M.R. Mumpower, G.C. McLaughlin, T.M. Sprouse, R. Surman, Coproduction of light and heavy r-process elements via fission deposition, Astrophys. J. 896 (2020) 28, https://doi.org/10.3847/1538-4357/ab91a9.
[47] S. Wanajo, The r-process in proto-neutron-star wind revisited, Astrophys. J. Lett. 770 (2013) L22, https://doi.org/10.1088/2041-8205/770/2/L22.
[48] M. Wang, W. Huang, F. Kondev, G. Audi, S. Naimi, The AME 2020 atomic mass evaluation (II). Tables, graphs and references, Chin. Phys. C 45 (2021) 030003, https://doi.org/10.1088/1674-1137/abddaf.
[49] N. Wang, M. Liu, X. Wu, J. Meng, Surface diffuseness correction in global mass formula, Phys. Lett. B 734 (2014) 215–219, https://doi.org/10.1016/j.physletb.2014.05.049.
[50] M.R. Wu, J. Barnes, G. Martínez-Pinedo, B.D. Metzger, Fingerprints of heavy-element nucleosynthesis in the late-time lightcurves of kilonovae, Phys. Rev. Lett. 122 (2019) 062701, https://doi.org/10.1103/PhysRevLett.122.062701, arXiv:1808.10459.
[51] D. Yong, C. Kobayashi, G.S. Da Costa, M.S. Bessell, A. Chiti, A. Frebel, K. Lind, A.D. Mackey, T. Nordlander, M. Asplund, A.R. Casey, A.F. Marino, S.J. Murphy, B.P. Schmidt, r-Process elements from magnetorotational hypernovae, Nature 595 (2021) 223–226, https://doi.org/10.1038/s41586-021-03611-2, arXiv:2107.03010.
[52] Y. Zhu, R.T. Wollaeger, N. Vassh, R. Surman, T.M. Sprouse, M.R. Mumpower, P. Möller, G.C. McLaughlin, O. Korobkin, T. Kawano, P.J. Jaffke, E.M. Holmbeck, C.L. Fryer, W.P. Even, A.J. Couture, J. Barnes, Californium-254 and kilonova light curves, Astrophys. J. Lett. 863 (2018) L23, https://doi.org/10.3847/2041-8213/aad5de, arXiv:1806.09724.
[53] Y.L. Zhu, K.A. Lund, J. Barnes, T.M. Sprouse, N. Vassh, G.C. McLaughlin, M.R. Mumpower, R. Surman, Modeling kilonova light curves: dependence on nuclear inputs, Astrophys. J. 906 (2021) 94, https://doi.org/10.3847/1538-4357/abc69e.